論文 / 著書情報
Article / Book Information

Title	Experimental investigation of the effects of adhesive thickness on the fracture behavior of structural acrylic adhesive joints under various loading rates
Authors	Yu Sekiguchi, Chiaki Sato
Citation	International Journal of Adhesion and Adhesives, Vol. 105, 102782
Pub. date	2020, 12
DOI	https://dx.doi.org/10.1016/j.ijadhadh.2020.102782
Creative Commons	See next page.
Note	This file is author (final) version.

License

Experimental investigation of the effects of adhesive thickness on the fracture behavior of structural acrylic adhesive joints under various loading rates

Yu Sekiguchi*, Chiaki Sato

Institute of Innovative Research, Tokyo Institute of Technology, 4259 Nagatsuta-cho, Midoriku Yokohama, 226-8503, Japan

Abstract

Designing joints requires a clear understanding of the appropriate thickness of the adhesive used. Structural acrylic adhesives have rarely been studied in terms of their thickness effect on the joint performance. To this end, the fracture resistance of a second-generation acrylic (SGA) adhesive was experimentally investigated by conducting a double cantilever beam (DCB) test. Because the SGA adhesive whitened when plastically deformed, the change of the plastic region with the crack growth was visualized. Therefore, the relationship between the fracture energy and the adhesive thickness was explained in terms of the plastically deformed area. With a thinner adhesive layer, the entire layer was whitened, and a linear relationship was obtained. In this region, the fracture energy increased from approximately 2 kJ/m^2 with an adhesive thickness of 0.2 mm to approximately 4 kJ/m^2 with 0.6 mm thickness. With more increase in the thickness, the fracture energy increased over 8 kJ/m^2. Increasing the thickness, however, resulted in partial whitening, yielding a non-linear relationship. Moreover, increasing the loading rate changed fracture behavior. At the opening speed of 2.5 m/s, stick-slip crack propagation was observed in any adhesive thickness, and the critical fracture energy dramatically decreased. In contrast, the arrest fracture energy under unstable crack propagation was independent of the loading rate and the adhesive thickness as approximately 1 kJ/m^2.

Keywords: structural acrylic, fracture toughness, impact loading, bond-line thickness

* Corresponding author. E-mail address: sekiguchi.y.aa@m.titech.ac.jp (Y. Sekiguchi)

1. Introduction

Nowadays, adhesive joints are widely used in many industries such as automotive, aerospace, and electronics. Owing to advantages, such as dissimilar material joining, damping improvement, and design flexibility, adhesive bonding technology has a significant potential to improve the functionality of products and is highly in demand. In particular, structural adhesives need to exhibit remarkably high strength and toughness to reliably bond load-bearing structures, and epoxies are often used as the base material of structural adhesives because of their excellent properties. With the development of materials, other types of polymers, such as polyurethane and acrylic resins, have also been applied as adhesives.

Second-generation acrylic (SGA) adhesives are two-component structural adhesives that can be rapidly cured at ambient temperatures [1-3]. A free-radical reaction occurs when two components, in which an oxidant and a reductant are contained separately, are mixed and the acrylic resin is polymerized. When the acrylic resin in adhesives is modified using an elastomer for toughening, a phase separation with a sea-island structure occurs [4, 5]. Because of the modulus difference between the sea and island areas, micro cracks and cavities are generated when plastically deformed. Thus, the adhesives whiten and fracture in a ductile manner. In addition, micro-fractures inside the adhesive layer inhibit adhesive failure at the interface and the SGA adhesives show superior cohesive failure performance. The SGA adhesives can fill gaps of a few millimeters and can be cured at room temperatures. Therefore, they are useful for on-site bonding, such as in repairing damaged parts and assembling large structures [3, 6, 7]. Moreover, they can be applied to functionally graded adhesive (FGA) joints [8, 9] by taking advantage of their mutability of flexibility.

The adhesive thickness is an important design parameter for adhesive joints, and its effects have been widely investigated, particularly on the fracture toughness [10-16]. Typically, the shear strength decreases with increasing adhesive thickness [15, 17]. In contrast, two types of relationships between the fracture energy and the adhesive thickness have been reported [18, 19]. With increasing the adhesive thickness, the fracture energy peaks and decreases to a certain value for brittle adhesives, whereas it increases and plateaus for ductile and tough adhesives [19]. The relationship in the case of brittle adhesives can be explained using the plastic zone diameter [20]. The fracture energy increases linearly when the plastic zone occupies the entire adhesive layer. It decreases and plateaus when the plastic zone diameter is smaller than the bond-line thickness. Conversely, a plateau appears even when the plastic zone occupies the entire adhesive layer in the case of ductile adhesives [19]. Because an accurate thickness control of adhesive layers is a difficult and time-consuming process in manufacturing sites, a clear understanding of how strictly the adhesive thickness must be controlled is important for joint design. The results reported in most studies are primarily for typical structural epoxy adhesives [10-14, 16, 18-20], while some are for polyurethane or silicone adhesives [15, 21-23]. The characteristics of adhesives significantly vary with the properties of the base polymers. Therefore, it is important to investigate the thickness effect for each type of adhesive.

Because adhesives are composed of polymers, they exhibit viscoelasticity, and the loading rate is another factor influencing the fracture toughness [20, 24-26]. In particular, for SGA adhesives, the glass transition temperature (Tg) of acrylic resins, such as polymethyl methacrylate (PMMA), is generally around 100 °C, and it decreases when modified with the elastomer. Thus, many SGA adhesives are sensitive to the operating environment.

In this study, the fracture behavior of a structural acrylic adhesive was investigated by measuring the mode I fracture energy of the adhesive using double-cantilever beam (DCB) tests. The effects of varying the loading rate, substrate thickness, and adhesive thickness on the fracture toughness were experimentally discussed.

2. Experimental

2.1 Specimens and materials

Two types of specimens with different substrate thicknesses were manufactured. There were two main reasons to change the substrate thicknesses; (1) to discuss the effect of the substrate rigidity on the plastic zone length at the crack tip and (2) to check the avoidance of the plastic deformation of the substrates. Because the rigidity of the substrate changes the stress state at the crack front, the plastically deformed area of the adhesive layer changes with substrate thickness. Therefore, by comparing the results at different substrate thicknesses, it is possible to determine whether the change in the fracture energy is affected not only by the adhesive thickness but also by the stiffness of the substrate. In addition, it was expected that the fracture energy was extremely increased when the adhesive thickness increased. If the substrate is plastically deformed, or if the experiment deviates significantly from the assumption of the DCB theory, the results at different substrate thicknesses should show totally different dependencies. Therefore, different geometrical specimens were prepared to confirm that it was not a peculiar change due to the shape of the test specimens. Figure 1 shows the specimen geometries, where h_{ad} is denoted as adhesive thickness. When the fracture energy is the same, the maximum stress applied to the substrate becomes higher with thinner substrate thickness. Therefore, in particular, for thin substrate specimens, it is important to avoid plastic deformation of the substrates, and steel with high yield stress was adopted as the substrate material. However, most of the high-strength steels in circulation have a thickness of a few millimeters or less. Therefore, it still had a possibility that the substrate plastically deformed when the adhesive thickness increased. Thus, the adhesively bonded area was narrowed following the method reported in [27]. With this method, it has been confirmed that the fracture energy can be measured in the same manner as the conventional method while the deformation of the substrate can be suppressed and the plastic deformation can be avoided.

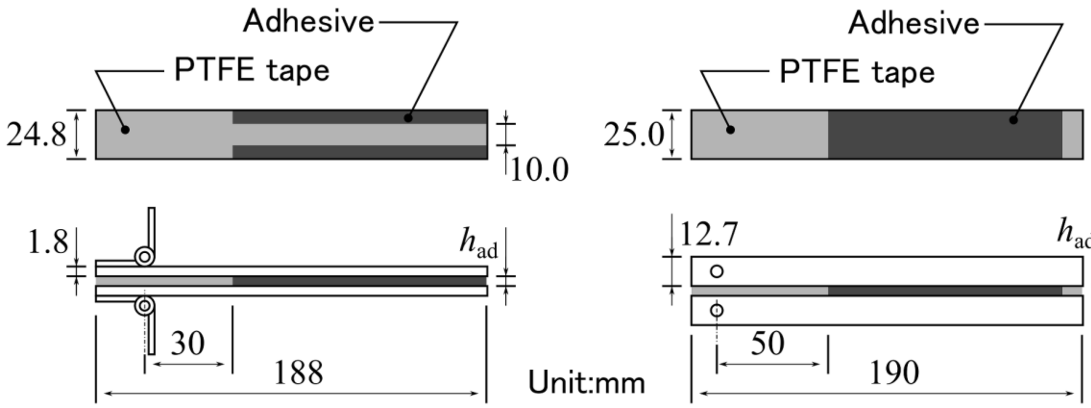

Fig. 1. Configuration and dimensions of thin- and thick-substrate DCB specimens. Above: Image of the adhesive layer (top view). Bottom: Image of the test specimen after bonded (side view).

The materials used in this study were a two-component acrylic adhesive (Hardloc C355-20 A/B, Denka Co., Ltd., Tokyo, Japan) and steels (carbon steel with the grade S50C for thick substrates and Cr-V-based spring steel with the grade SUP10 for thin substrates). The spring steel has a high yield strength of over 1080 MPa, whereas it is over 365 MPa for the S50C steel (values were provided from the manufacturers). The commonly used Young's modulus value for steel (206 GPa) was used for the calculation in this study. The Young's modulus, Poisson's ratio, and Tg of the adhesive were experimentally obtained as 300 MPa, 0.37, and 87 °C, respectively [26, 28]. Figure 2 shows the stress–strain relationships of the bulk and cylindrical butt joint specimens [28]. The restraint of the thin adhesive layer by the adherend for the butt joint could be the reason for the high yield stress and the damaged region with stress reduction, which are the major difference from the bulk results.

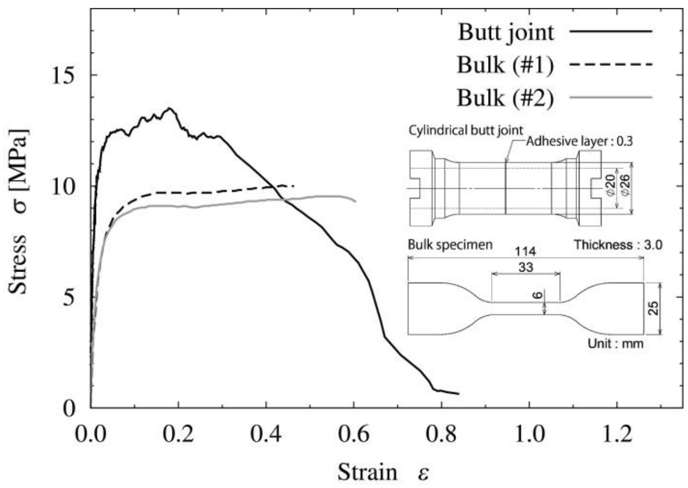

Fig. 2. Stress–strain diagrams from tensile tests conducted on cylindrical butt joint and bulk specimens [28].

The manufacturing process was the same for both the specimen geometries. First, the surfaces of the substrate were sandblasted with an Al_2O_3 grit (SG-118-120 Grid #120, Hozan Tool Ind. Co., Ltd., Osaka, Japan) as an abrasive medium. The sandblasted surface had the surface roughness of Ra ≈ 1.0 μm, Rz ≈ 7.0 μm, and RSm ≈ 70 μm. After the abrasive sand was removed using high-pressure air and wipes, the substrate thickness was measured. The surfaces were wiped with ethanol prior to the bonding. The adhesive thickness was controlled by inserting polytetrafluoroethylene (PTFE) tapes. After the substrates were bonded, they were cured for 24 h at room temperature (24±2 °C). Subsequently, they were placed in an electric furnace at 60 °C for 2.5 h as a post-curing treatment, and the overflowing adhesives were peeled off using an ultrasonic cutter. The specimen thickness was measured after the manufacturing process, and the adhesive thickness was calculated by subtracting the substrate thickness from the overall specimen thickness.

2.2 DCB tests using universal testing machines

DCB tests were conducted on the universal testing machine STB-1125S (A&D Co., Ltd., Tokyo, Japan) with a load cell capacity of 500 N for the thin substrate specimens and on AG-X (Shimadzu Co., Ltd., Kyoto, Japan) with a load cell capacity of 50 kN for the thick substrate specimens. The crack length was measured using a CMOS camera installed to observe the specimens from the side. To deduce the critical fracture energy G_c, the corrected beam theory (CBT) was applied [29].

$$G_c = \frac{3P\delta F}{2b(a+|\Delta|)} \quad (1)$$

where P is the load, δ is the displacement, b is the width of the bonded area, a is the crack length, and F is the displacement correction factor, which is described as follows [30].

$$F = 1 - \frac{3}{10}\left(\frac{\delta}{a}\right)^2 - \frac{3}{2}\left(\frac{l_1\delta}{a^2}\right) \quad (2)$$

where l_1 is the distance from the load point to the substrate axis. In the case of extremely high G_c value with the thin substrate, the substrate with the non-adhered area largely bend and the length of the cantilever part becomes not equal to the crack length. The correction factor F corrects this discrepancy. The crack length correction $|\Delta|$ was obtained from the relationship between $C^{1/3}$ and a, where $C = \delta/P$ is the compliance. In order to avoid the R-curve effect, G_c values for initiation were not evaluated and the data of $a > a_0 + 15$ mm, i.e., G_c values for propagation, was used for the calculation of stably propagated results. In addition to the crack length measurement, the length from the load point to the whitening front a_w (see Fig. 3) was optically measured and the whitening length $a_w - a$ was obtained. Furthermore, the equivalent crack length a_e was calculated from the load and displacement using the equation

$$a_e = \left(\frac{3EI\delta}{2P}\right)^{1/3} \quad (3)$$

based on the beam theory, where E is the substrate modulus and I is the moment of inertia of the substrate cross-section. The shear effect on the beam deflection was less than 1% and therefore neglected. The original DCB theory is based upon liner elastic fracture mechanics (LEFM). However, the adhesives largely plastically deform at the crack front. In the case when the adhesive exhibits elasto-plasticity like the SAG adhesives, it has been confirmed by extending the Winkler model and performing elasto-plastic analysis that the fracture energy can be correctly calculated by the CBT [31]. In this case, the crack length correction contains not only the rotation effect of the substrate but also the plastically deformed length of the adhesive layer. Additionally, the equivalent crack length is known to predict the point where the substrate starts bending when the adhesive exhibits elasto-plasticity [31]. Therefore, the length $a_e - a$ also predicts the deformed length of the adhesive layer, including both elastic and plastic deformations, and it is later compared with $a_w - a$ and $|\Delta|$. In the case of an unstable fracture, the fracture energy is determined using the Timoshenko beam theory as

$$G = \frac{P^2F}{3EIb}(3a_e^2 + h^2) \quad (4)$$

which is the so-called compliance-based beam method (CBBM), where h is the substrate thickness.

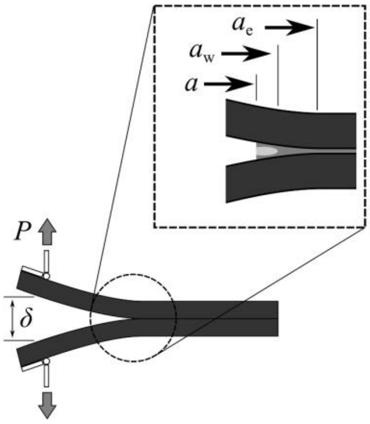

Figure 3 Schematic of the crack front, whitening front, and equivalent crack front.

2.3 DCB tests using a drop weight impact test machine

Impact DCB tests were conducted using a drop-weight-type impact testing machine [24]. Specimens with a thin substrate were used. Wedges were set on the weights to open the specimens, as shown in Fig. 4. The displacement and crack length were obtained from the images recorded using a high-speed camera (CRYSTA PI-IPS, Photron Co., Ltd., Tokyo, Japan). Because the load was not recorded during the impact tests, the load expressed in Eq. (1) was replaced with the displacement and crack length using the simple beam theory. Thus, the fracture energy can be represented as a function of δ and a as [26]:

$$G = \frac{9\delta^2 EIF}{4b(a+|\Delta|)^4} \quad (5)$$

Because the substrate was thin enough to neglect the kinetic energy of the substrate, the dynamic effect on the fracture energy was not considered.

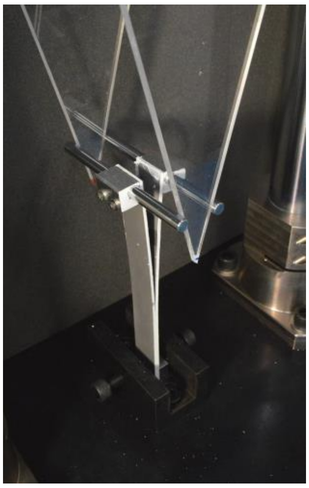
Fig. 4. Image of specimen opening for impact DCB tests [24].

3. Results and discussions

3.1 DCB tests using universal testing machines

Universal testing machines were used to carry out a series of DCB tests on two substrates with different thicknesses, as described previously, by varying the adhesive thickness. In all the configurations, a cohesive fracture was observed.

First, quasi-static tests with an obtuse-angle initial crack (type 1, as shown in Fig. 5a) were conducted. The displacement speed was set to 1 mm/min for the thick substrate specimen and 5 mm/min for the thin substrate specimen. Similar relationships between the critical fracture energy and the adhesive thickness were obtained regardless of the substrate thickness, as shown in Fig. 6. The fracture energy increased from approximately 2 kJ/m^2 to over 6 kJ/m^2. The solid line in the figurer indicates the least-square fit of the results for h_{ad} < 0.6 mm, which is also plotted in the other results for reference. The lengths $a_{\mathrm{w}} - a$ and $a_{\mathrm{e}} - a$ were different depending on the substrate thickness. The average value of $a_{\mathrm{w}} - a$ was 7.8±1.1 mm for the thin substrate specimen and 29.5±4.3 mm for the thick substrate specimen; the $a_{\mathrm{e}} - a$ values were 11.2±0.8 and 32.5±4.1 mm, respectively. The length was longer for substrates with a high bending rigidity, but it was more than twice the adhesive thickness even for the thin substrate specimen. Therefore, the process zone in the longitudinal direction was large enough relative to the adhesive thickness. In addition, the equivalent crack front was always a few millimeters ahead of the whitening front. In other words, $a_{\mathrm{e}} - a_{\mathrm{w}}$ expresses the elastically deformed length of the adhesive layer.

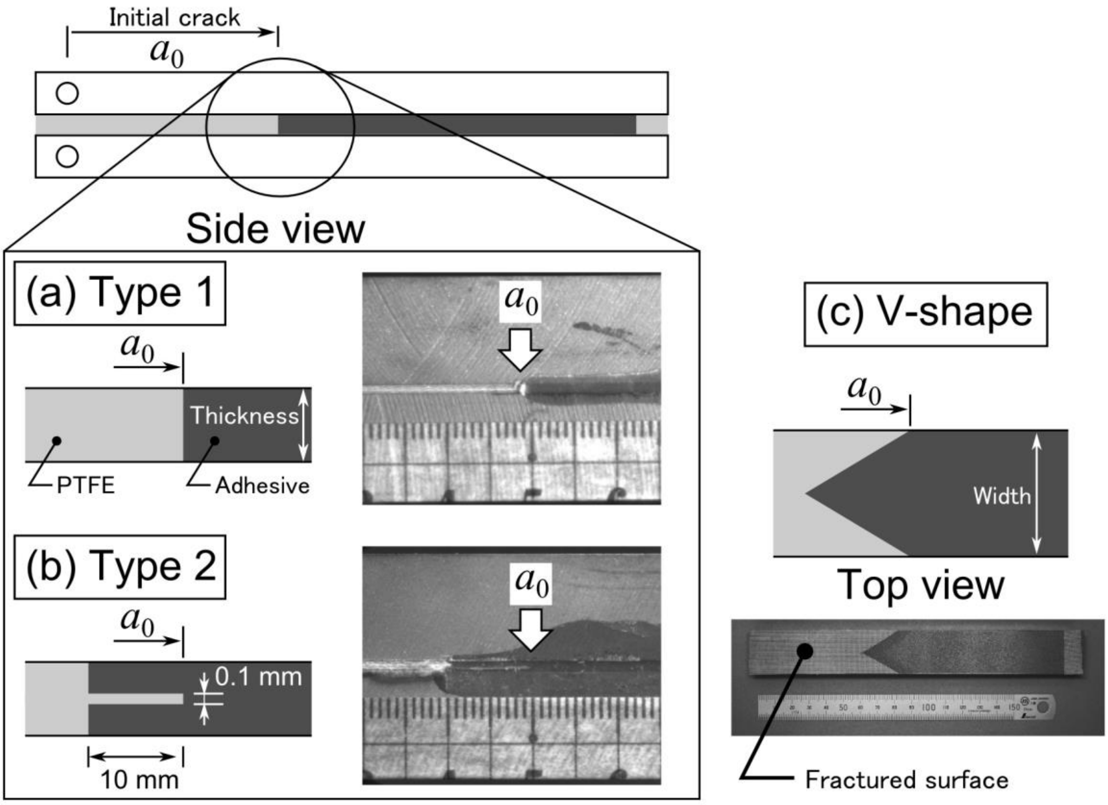

Fig. 5. Schematics of initial crack configurations: (a) obtuse angle (type 1), (b) acute angle (type 2), and (c) V-shape.

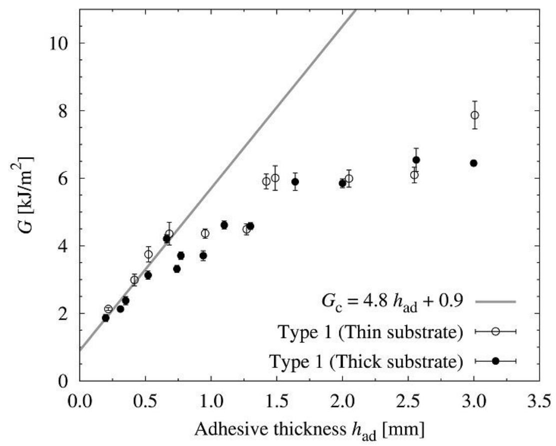

Fig. 6. Adhesive fracture energy as a function of the adhesive thickness for an obtuse-angle initial crack under the quasi-static condition.

Because the SGA adhesive was highly ductile, the crack propagated through the center of the adhesive layer in the case of the thin layer even with the obtuse-angle initial crack, as shown in Fig. 7a. With increasing the adhesive thickness, however, the crack position varied and it propagated along with the interface, as shown in Fig. 7b. This change was observed when h_{ad} was greater than approximately 0.7 mm. As a result, the plastic deformation was limited to a part of the adhesive layer. This partial energy consumption led to nonlinearity. Introducing an acute-angle initial crack (type 2, as shown in Fig. 5b) led to a dramatic change in the whitening area for the thicker adhesive layer, as shown in Fig. 7c. The linear region expanded to approximately twice the size, as shown in Fig. 8. A clear difference can be observed, particularly for the thick substrate specimens. The fracture energy for type 2 with thicker adhesive layer was increased over 8 kJ/m^2. However, cracks started propagating once again near the interface when h_{ad} exceeded approximately 2 mm, and a nonlinear relationship was observed. In contrast, the whitening length in the longitudinal direction was not affected by the adhesive thickness and the crack position, as shown in Fig. 9. Therefore, the whitening occupancy in the thickness direction was an important factor influencing the linear relationship between the fracture energy and the adhesive thickness.

Because the geometry of the thin and thick substrates is different, the amount of plastic energy should be different even if the substrate plastically deforms. Therefore, the existence of plastic deformation can be confirmed by comparing the results. Visually no plastic deformation was observed for both the thin and thick substrates in all cases, but the difference was observed at $h_{\mathrm{ad}} = 3.0$ for type 1, as shown in Fig. 6, which may have a possibility to contain some plastic deformation for the thin substrate. Conversely, no large difference was observed for type 2 comparing the thin and thick results. Therefore, it was confirmed that, in most cases, the plastic deformation was avoided for the tested configuration.

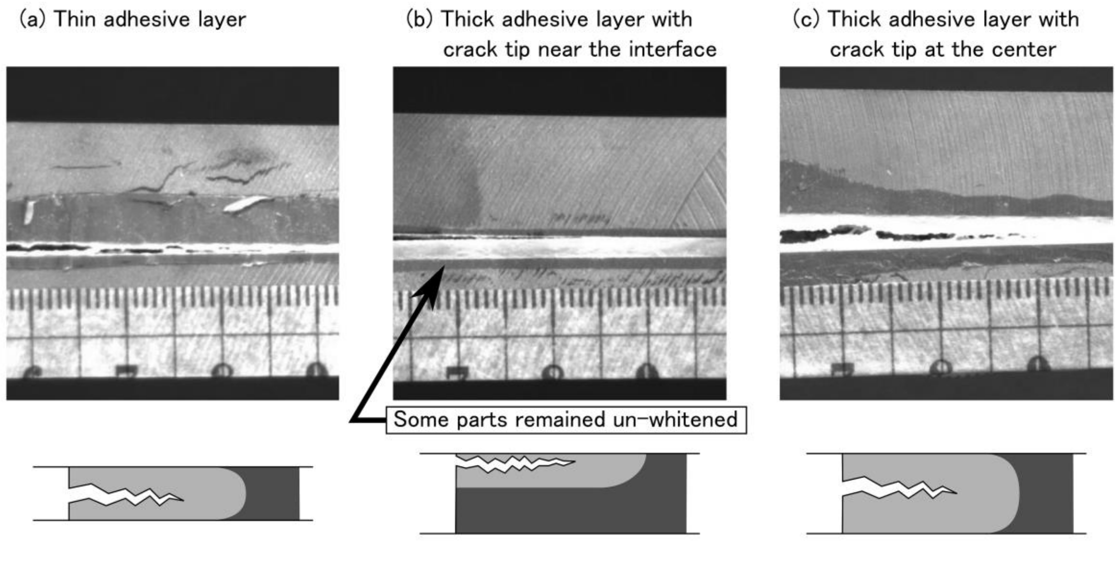

Fig. 7. Enlarged images of the crack front for (a) thin adhesive layer, (b) thick adhesive layer with a

crack tip near the interface, and (c) thick adhesive layer with a crack tip at the center.

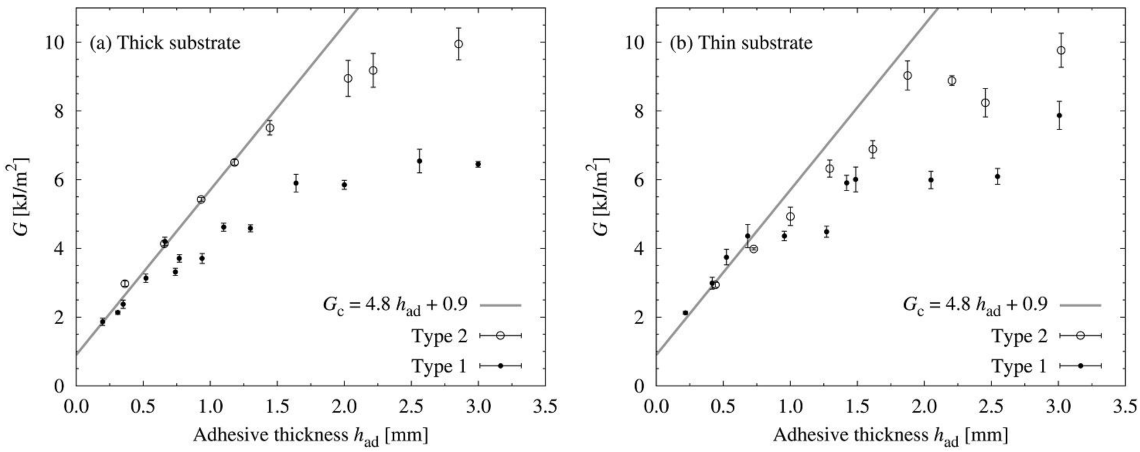

Fig. 8. Adhesive fracture energy as a function of adhesive thickness under the quasi-static condition with a difference in the initial crack for (a) thick substrate specimen and (b) thin substrate specimen.

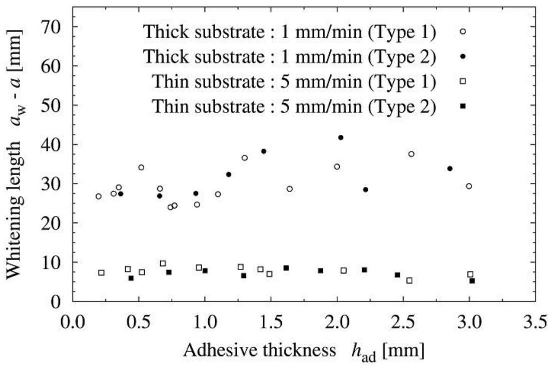

Fig. 9. Whitening length versus adhesive thickness under quasi-static condition.

As the loading rate increased, the fracture became unstable, particularly for the thicker adhesive layer. In the case of the thick substrate specimens, unstable crack propagation was observed for most adhesive thicknesses when the displacement speed was increased to the maximum machine speed of 0.5 m/min, as shown in Fig. 10a. When the crack propagated unstably, the maximum G value calculated with CBBM was used as the G_c value for initiation. The strain rate is much higher at crack initiation than during propagation in the case of DCB tests with elastic–plastic adhesives [31]. Thus, the unstable crack propagation may be avoided if the crack is gradually initiated at the beginning. Therefore, a V-shaped initial crack (Fig. 5c) was introduced, and a stable crack propagation could be observed over a wide range of adhesive thicknesses, as shown in Fig. 10b. In addition, the crack propagation was stable when the displacement speed was slightly decreased to 0.3 m/min, as shown in Fig. 11. At the same time, the deviation between types 1 and 2 became small enough to be indistinguishable. A similar change was also observed in the case of the thin substrate specimens. The deviation between types 1 and 2 can hardly be seen when increasing the displacement speed to 0.1 m/min, as shown in Fig. 12. With the machine speed increased to a maximum of 1 m/min, unstable crack propagation was observed for the thicker adhesive layer, as shown in Fig. 13. When unstable cracks propagated in the thick substrate specimens, the load decreased as the cracks extended, because the specimen length was too short to permit crack arrest (Fig. 14a). Therefore, only the fracture energy at the beginning of crack initiation was obtained. In contrast, in the thin substrate specimens, the cracks arrested, and stick-slip propagation or initial slip and then stable propagation was observed (Fig. 14b). Thus, the arrest fracture energy G_a was also obtained.

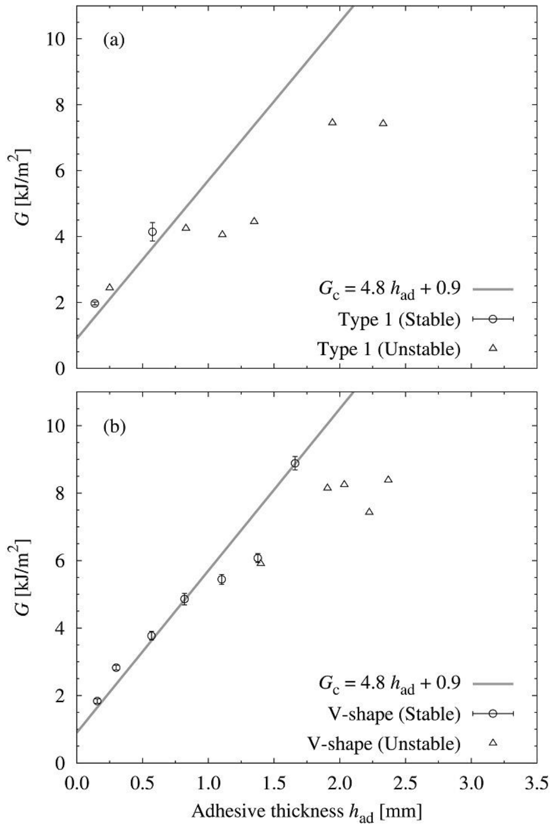

Fig. 10. Adhesive fracture energy as a function of adhesive thickness for a thick substrate specimen with a loading rate of 0.5 m/min.

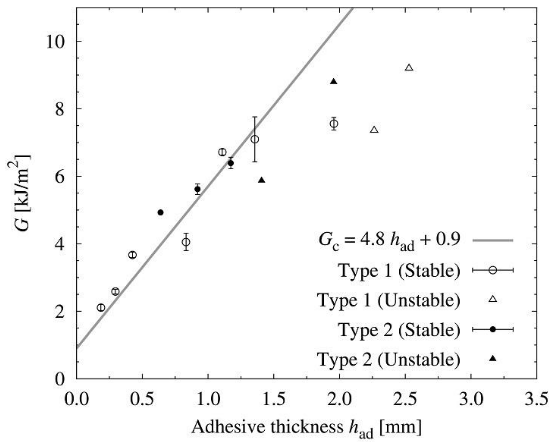

Fig. 11. Adhesive fracture energy as a function of adhesive thickness for a thick substrate specimen with a loading rate of 0.3 m/min.

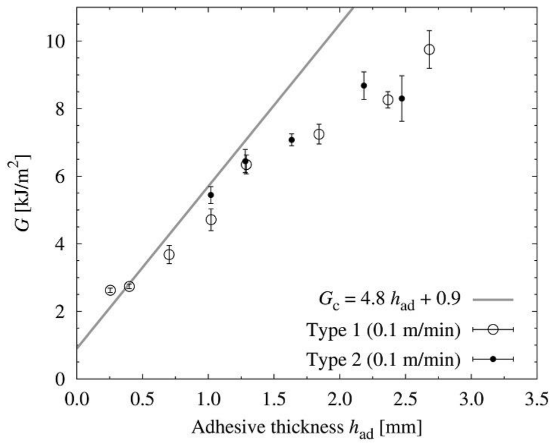

Fig. 12. Adhesive fracture energy as a function of adhesive thickness for a thin substrate specimen with a loading rate of 0.1 m/min.

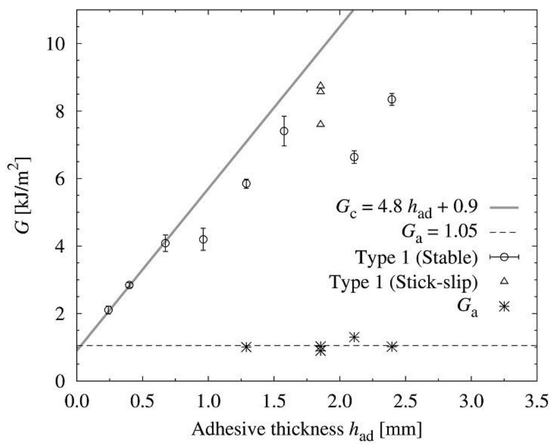

Fig. 13. Adhesive fracture energy as a function of adhesive thickness for a thin substrate specimen

with a loading rate of 1 m/min.

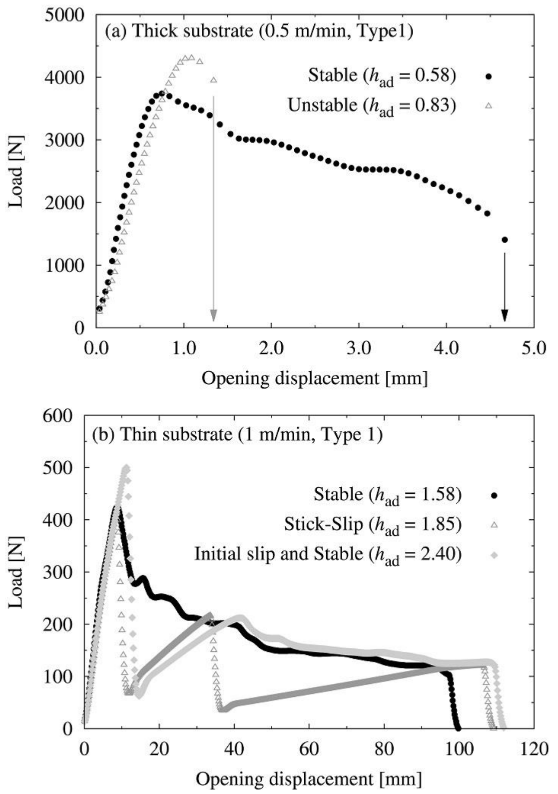

Fig. 14. Load–displacement relationship for (a) thick substrate specimen and (b) thin substrate specimen.

3.2 DCB tests using an impact test machine

Impact DCB tests were conducted on the thin substrate specimens using a drop-weight impact test machine. The displacement speed was calculated from the images. It was found to be approximately 0.7 m/s when the weight was released from the lowest start position and approximately 2.5 m/s from the highest. In all the configurations, a cohesive fracture was observed.

The crack length correction $|\Delta|$ is essential to calculate the fracture energy in impact DCB tests. Although the load, displacement, and crack length should be measured to obtain $|\Delta|$ in CBT, the load was not measured in the impact tests in this study. Thus, it cannot be determined directly. From the results obtained using the universal testing machine, $|\Delta|$ was found to be largely between $a_e - a$ and $a_w - a$, as shown in Fig. 15. However, the load was also used to determine a_e. Thus, $a_e - a$ cannot be calculated in the impact tests either. Fortunately, $a_e - a$ seems to be less independent on the loading rate. Therefore, the average $a_e - a$ value (10.7 mm) and optically measured $a_w - a$ at each displacement speed were used to calculate the critical and arrest fracture energies, as shown in

Figs. 16 and 17. The solid line and dashed-dotted line indicate the least-squares fitted lines of G_c obtained using $|\Delta| = a_w - a$ and $|\Delta| = a_e - a$, respectively. Although the exact value cannot be determined because of the above reasons, the actual fracture energies were expected to be between these values. The dashed line indicates the average value of G_a. At both the displacement speeds, stick-slip crack propagation was observed.

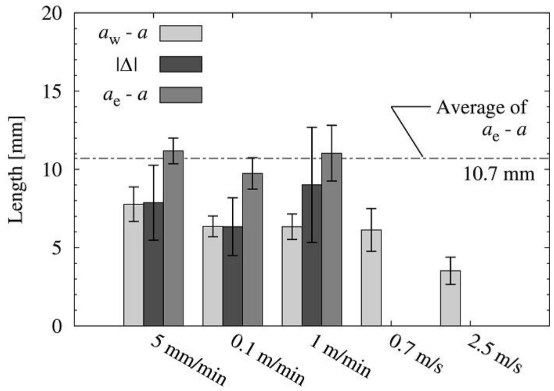

Fig. 15. Mean values of $a_w - a$, $|\Delta|$ and $a_e - a$ for the thin substrate specimens at each loading rate.

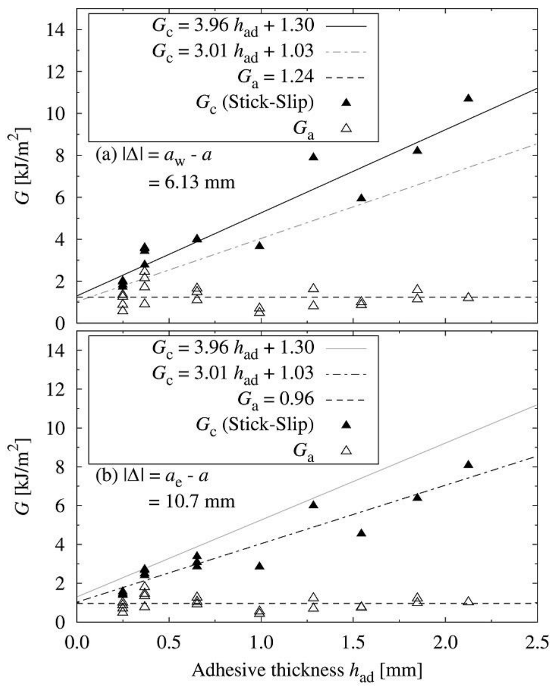

Fig. 16. Adhesive fracture energy as a function of adhesive thickness for a thin substrate specimen with a loading rate 0.7 m/s calculated using (a) $|\Delta| = a_w - a$ and (b) $|\Delta| = a_e - a$.

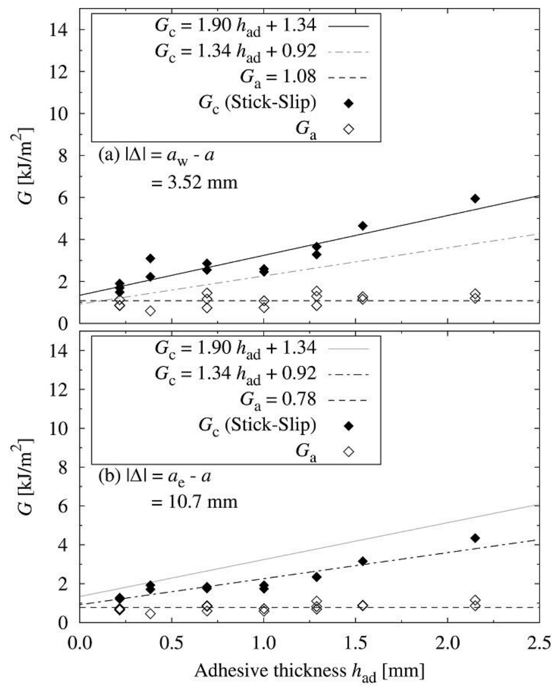

Fig. 17. Adhesive fracture energy as a function of adhesive thickness for a thin substrate specimen with a loading rate 2.5 m/s calculated using (a) $|\Delta| = a_{\mathrm{w}} - a$ and (b) $|\Delta| = a_{\mathrm{e}} - a$.

In the case of the stick-slip crack propagation, whitening was only generated when the crack was stuck, as shown in Fig. 18a. Because the energy consumed by the plastic deformation was related to the size of the whitened area, the critical fracture energy decreased in accordance with the decrease in the whitening length accompanying the increase in the loading rate (see Fig. 19). In contrast, G_{a} maintained a constant value regardless of the test conditions. During unstable crack propagation, no whitening was observed, as shown in Fig. 18b. Thus, a narrow process zone was expected around the crack tip when the crack was arrested, and G_{a} was not affected by the adhesive thickness. In addition, the unstable crack velocity was largely constant at approximately 20 m/s, as shown in Fig. 20. Therefore, G_{a} was also independent of the loading rate.

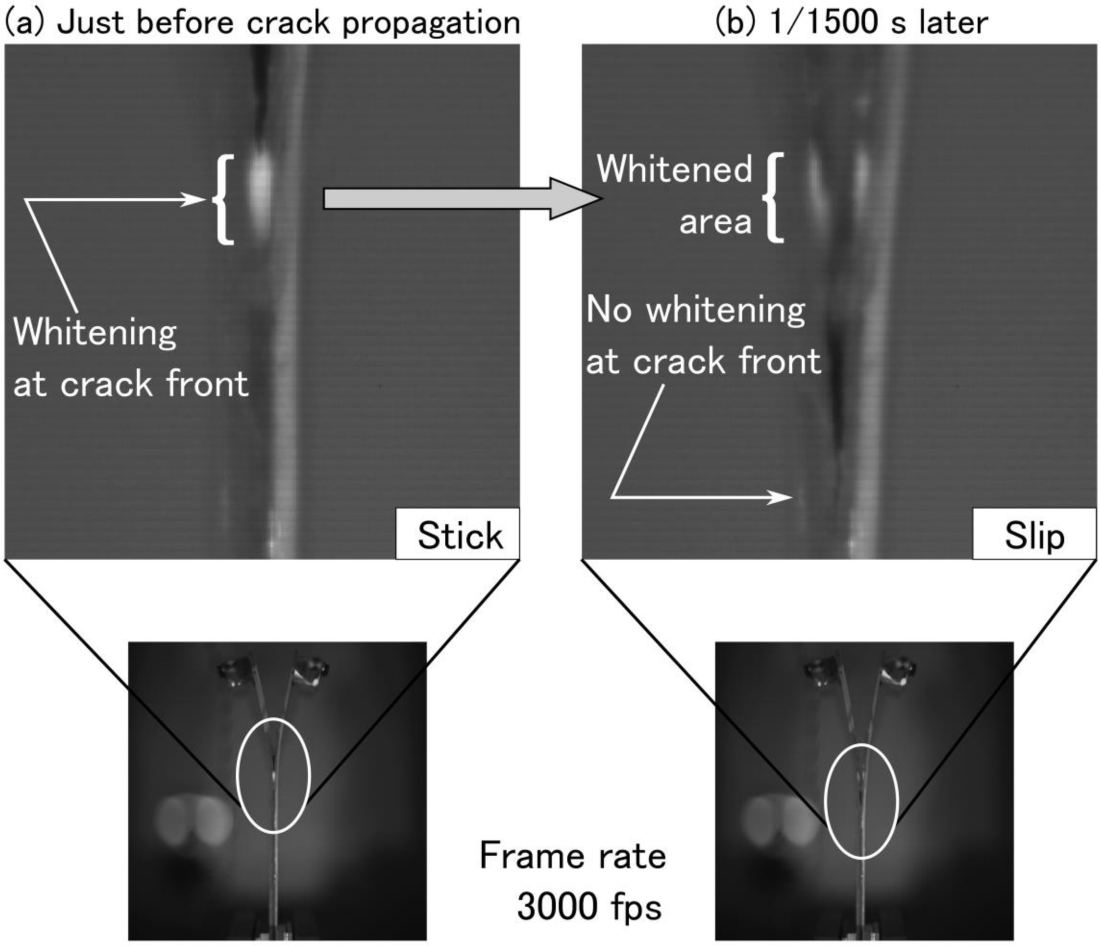

Fig. 18. Images of stick-slip propagation under impact loading.

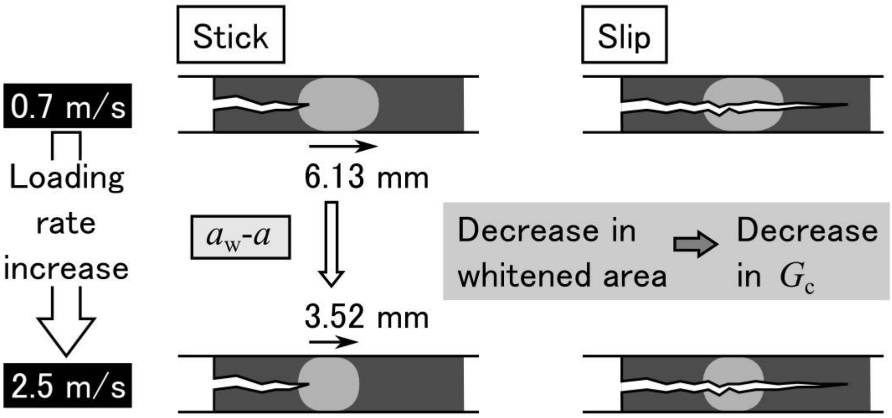

Fig. 19. Schematics of the transition of the whitened area under impact loading.

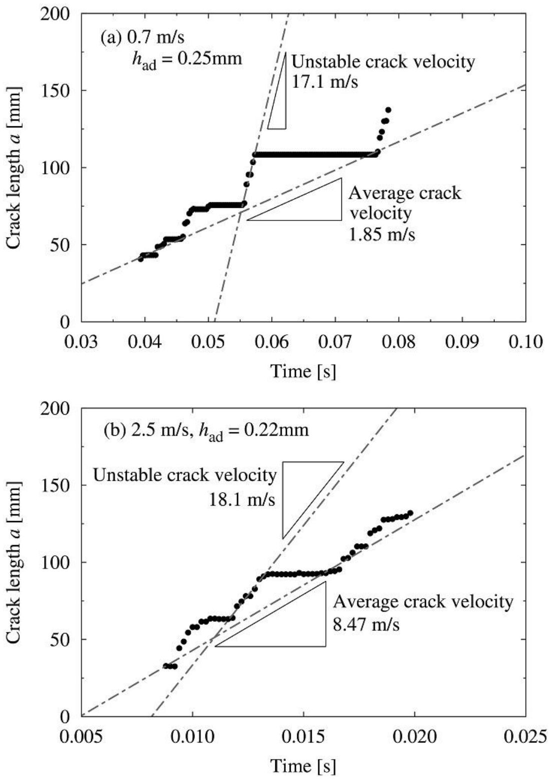

Fig. 20. Determination of the average crack velocity and unstable crack velocity for a stick-slip crack growth from the crack length versus time plot. (Examples shown are for the loading rate and the adhesive thickness for (a) 0.7 m/s and 0.25 mm, (b) 2.5 m/s and 0.22 mm, respectively.)

3.3 Loading rate effect

Figure 21 shows the overall trend in the relationship between the fracture behavior and the adhesive thickness. The relationship was divided into three phases based on the loading rate. With stable crack propagation under quasi-static conditions, linear and nonlinear relationships were observed depending on the presence of plastic deformation in the adhesive layer (first phase). When increasing the loading rate, a transition from stable to unstable crack propagation was observed (second phase). This occurred particularly when the adhesive layer was thicker. Under the impact loading condition, the cracks propagated unstably at all adhesive thicknesses, and G_c decreased with increasing loading rate, whereas G_a remained constant (third phase). The crack velocity increased with increasing opening displacement speed; however, the unstable crack velocity remained largely constant, as shown in Fig. 22. With a further increase in the loading rate, the average crack velocity of the stick-slip propagation could reach the unstable crack velocity. Therefore, another phase is expected when it reaches a much higher opening displacement speed; this remains to be future work. Figure 23 shows the fracture energy against the opening displacement speed with several selected adhesive thicknesses. Overall, the fracture energy tends to decrease as the speed increases, but it can be seen that the thicker the thickness, the greater the change.

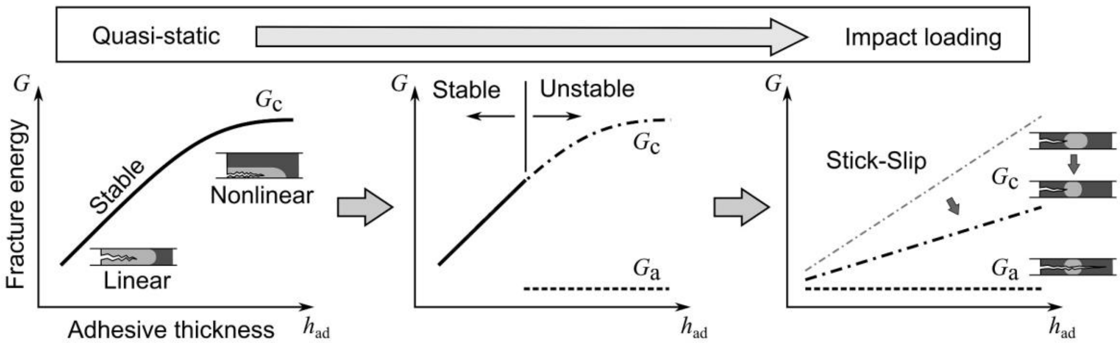

Fig. 21. Schematic model for explaining the relationship between the adhesive fracture behavior and the adhesive thickness with varying loading rates.

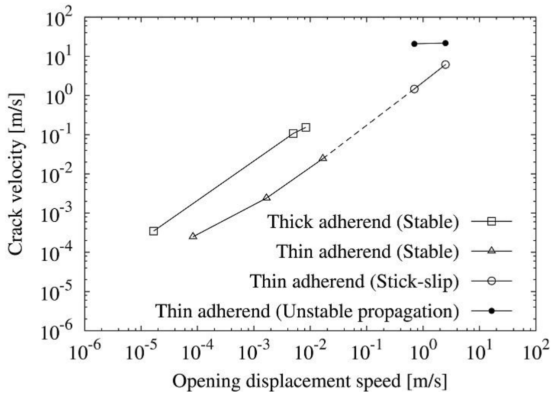

Fig. 22. Crack velocity versus opening displacement speed.

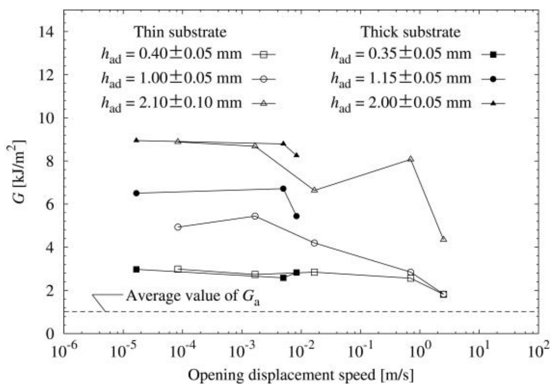

Fig. 23. Fracture energy versus opening displacement speed for several adhesive thicknesses.

3.4 Fracture energy partition

Pardoen et al. [32] proposed the adhesive fracture energy concept, where the fracture energy is divided into two components: the intrinsic work of the fracture associated with the cohesive zone, G_0, and the additional contribution to the adhesive fracture toughness arising from the far-field plastic dissipation and stored elastic energy within the adhesive layer, G_p, as $G_c = G_0 + G_p$. Additionally, G_0 was assumed to be independent of the adhesive thickness. Thus, the effect of the adhesive thickness on the fracture energy was only included in G_p. Depending on the type of adhesive, several other approaches have also been considered [14], and determining the concept that matches the results requires a case-by-case analysis, particularly depending on the toughening mechanisms of the adhesive.

When elastomer-toughened acrylic adhesives are cured, the phase separation generates a random distribution of the elastomer particles in the acrylic resin [4], and an elastomer-rich area and an acrylic-rich area are formed [5]. The micro/nanoscale modulus distribution causes a complex and random stress state. Thus, cavities and microcracks are generated, which are considered key to the toughening mechanisms of structural acrylic adhesives. A detailed observation of the fracture surface revealed that the cracks propagated along the brittle part, i.e., the acrylic-rich area, whereas the ductile part, i.e., the elastomer-rich area, around the cracks was largely plastically deformed [33]. Applying Pardoen's concept, the former crack growth is associated with G_0 and the latter plastic deformation is associated with G_p. For an unstable crack propagation, the plastic deformation effect almost disappears, and the fracture energy that is independent of the loading rate and adhesive thickness becomes dominant. Therefore, $G_\mathrm{p} \approx 0$ and $G_0 = G_\mathrm{a}$. In contrast, the fracture energy for a stable crack propagation has both effects. However, the fracture energy is asymptotic to G_a when the adhesive thickness approaches zero because G_p is zero at zero thickness. Therefore, $G_0 = G_\mathrm{a}$, i.e., $G_\mathrm{p} = G_\mathrm{c} - G_\mathrm{a}$, is also assumed when the cracks propagate stably. In the case of the adhesive used in this study, load-independent fracture energy (fracture energy in arrest) was approximately 1 kJ/m^2 and zero thickness fracture energy (intercept of the least-square fit) was approximately 0.9 kJ/m^2, and both values were very close. Therefore, G_0 should be around these values and the rest of the energy was dissipated by the plastic deformation around the crack tip.

The slope of the relationship between the fracture energy and the adhesive thickness expresses the change in the energy consumption per volume with increasing adhesive thickness. The slope in the linear region of the quasi-static DCB tests was approximately 4800 kJ/m^3, which corresponds to $G_\mathrm{p}/h_\mathrm{ad}$. From the tensile test results shown in Fig. 2, the energy consumed per volume under plastic deformation, i.e., the area under the stress–strain curve, was found to be approximately 5000 kJ/m^3 for the bulk specimen and approximately 7000 kJ/m^3 for the cylindrical butt joint specimen. A value similar to the energy consumption per volume from the tensile tests confirmed that the increase in the fracture energy with increasing adhesive thickness was mainly related to the plastic energy dissipation in the adhesive layer.

4. Conclusion

Double cantilever beam tests were conducted to investigate the bond-line thickness effect on the adhesive fracture energy of a second-generation acrylic (SGA) adhesive. The adhesive used in the experiment was highly ductile and whitening was observed when plastically deformed. Therefore, the plastically deformed area at the crack front was visualized and a change in the process zone with varying the adhesive thickness, loading rate, and substrate thickness was clarified. Under the quasi-static condition, the fracture energy linearly increased with the adhesive thickness when the entire layer was whitened. However, when the thickness was increased, the crack position moved near the interface, partial whitening was observed, and the linearity was lost. Increasing the loading rate, unstable crack propagation was observed for a thicker adhesive layer and transitioned to stick-slip crack propagation at all adhesive thicknesses under the impact loading condition. Furthermore, for the stick-slip crack propagation, a decrease in the whitened area with an increase in the loading rate led to a decrease in the critical fracture energy. In contrast, the arrest fracture energy was independent of the loading rate and adhesive thickness. Moreover, the critical fracture energy was asymptotic to the arrest fracture energy when the adhesive thickness approached zero. Therefore, it was concluded that the change in the fracture energy of the SGA adhesive with the adhesive thickness is mainly attributed to the plastic energy dissipation around the crack tip, and the intrinsic work of fracture remains constant. However, it was also revealed that the whitening area significantly changed with the initial crack condition and substrate rigidity. Therefore, careful discussion is required when analyzing the fracture behavior of actual structures.

Acknowledgements

This work was based on results obtained from a project commissioned by the New Energy and Industrial Technology Development Organization (NEDO). We also would like to thank Cactus Communications for English language editing.

References

1. Allen KW, Harzinikolaou T, ArmstrongKB. A comparison of acrylic adhesives for bonding aluminium alloys after using various surface preparation methods. Int J Adhes Adhes 1984;4(3):133-6. http://doi.org/10.1016/0143-7496(84)90015-0
2. Dodiuk H, Kenig S. The effect of surface preparation on the performance of acrylic adhesive joints. Int J Adhes Adhes 1988;8(3):159-66. http://doi.org/10.1016/0143-7496(88)90094-2
3. Suto H, Yoda K, Watanabe J, Yang L. Development of the low-odor and non-flammable second-generation acrylic adhesive and its applications. J Adhes Soc Jpn 2012;48(4):127-36. http://doi.org/10.11618/adhesion.48.127
4. Kamiyama K, Mikuni M, Matsumoto T. Fracture propagation analysis on two component type acrylic adhesive joints. Int J Adhes Adhes 2018;83:76-86. http://doi.org/10.1016/j.ijadhadh.2018.02.019
5. Hayashi A, Sekiguchi Y, Sato C. AFM observation of sea-island structure formed by second generation acrylic adhesive. J Adhes, in press. http://doi.org/10.1080/00218464.2019.1649148
6. Haraga K, Taguchi K, Yoda K, Nakashima Y. Assembly technique for control panel enclosures with the combined use of adhesive and rivets and the reduction of energy consumption. Int J Adhes Adhes 2003;23:371-6. http://doi.org/10.1016/S0143-7496(03)00066-6
7. Iwata T, Hayashibara H. Durability and flammability evaluation of SGA structural adhesive joints consisting of a thick adhesive layer for shipbuilding. J Adhes 2019;95(5-7):614-31. http://doi.org/10.1080/00218464.2019.1581067
8. Nakanouchi M, Sato C, Sekiguchi Y, Haraga K, Uno H. Development of application method for fabricating functionally graded adhesive joints by two-component acrylic adhesives with different elastic moduli. J Adhes 2019;95(5-7):529-42. http://doi.org/10.1080/00218464.2019.1583562
9. Sekiguchi Y, Nakanouchi M, Haraga K, Takasaki I, Sato C. Experimental investigation on strength of stepwise tailored single lap adhesive joint using second-generation acrylic adhesive via shear and low-cycle shear tests. In J Adhes Adhes 2019;95:102438. http://doi.org/10.1016/j.ijadhadh.2019.102438
10. Ji G, Ouyang Z, Li G, Ibekwe S, Pang SS. Effects of adhesive thickness on global and local mode-I interfacial fracture of bonded joints. Int J Solids Struct 2010;47:2445-58. http://doi.org/10.1016/j.ijsolstr.2010.05.006
11. Da Silva LFM, de Magalhães FACRG, Chaves FJP, de Moura MFSF. Mode II fracture toughness

of a brittle and a ductile adhesive as a function of the adhesive thickness. J Ades 2010;86:891-905. http://doi.org/10.1080/00218464.2010.506155

12. Marzi S, Biel A, Stigh U. On experimental methods to investigate the effect of layer thickness on the fracture behavior of adhesively bonded joints. Int J Adhes Adhes 2011;31:840-50. http://doi.org/10.1016/j.ijadhadh.2011.08.004
13. Khoo TT, Kim H. Effect of bondline thickness on mixed-mode fracture of adhesively bonded joints. J Adhes 2011;87:989-1019. http://doi.org/10.1080/00218464.2011.600868
14. Cooper V, Ivankovic A, Karac A, McAuliffe D, Murphy N. Effects of bonded gap thickness on the fracture of nano-toughened epoxy adhesive joints. Polymers 2012;53:5540-53. http://doi.org/10.1016/j.polymer.2012.09.049
15. Banea MD, da Silva LFM, Campilho RDSG. The effect of adhesive thickness on the mechanical behavior of a structural polyurethane adhesive. J Adhes 2015;91:331-46. http://doi.org/10.1080/00218464.2014.903802
16. Han X, Jin Y, da Silva LFM, Costa M, Wu C. On the effect of adhesive thickness on mode I fracture energy -an experimental and modelling study using a trapezoidal cohesive zone model. J Adhes 2020;96(5):490-514. http://doi.org/10.1080/00218464.2019.1601087
17. Arenas JM, Narbón JJ, Alía C. Optimum adhesive thickness in structural adhesives joints using statistical techniques based on Weibull distribution. Int J Adhes Adhes 2010;30:160-5. http://doi.org/10.1016/j.ijadhadh.2009.12.003
18. Lee DB, Ikeda T, Miyazaki N, Choi NS. Effect of bond thickness on the fracture toughness of adhesive joints. Trans ASME 2004;126:14-18. http://doi.org/10.1115/1.1631433
19. Quan D, Murphy N, Ivankovic A. Fracture behavior of epoxy adhesive joints modified with core-shell rubber nanoparticles. Eng Fract Mech 2017;182:566-76. http://doi.org/10.1016/j.engfracmech.2017.05.032
20. Kinloch AJ, Shaw SJ. The fracture resistance of a toughened epoxy adhesive. J Adhes 1981;12:59-77. http://doi.org/10.1080/00218468108071189
21. Boutar Y, Naïmi S, Mezlini S, da Silva LFM, Ali MBS. Characterization of aluminium one-component polyurethane adhesive joints as a function of bonded thickness for the automotive industry: Fracture analysis and behavior. Eng Fract Mech 2017;177:45-60. http://doi.org/10.1016/j.engfracmech.2017.03.044
22. Manterola J, Cabello M, Zurbitu J, Renart J, Turon A, Jumel J, Urresti I. Effect of the width-to-

thickness ratio on the mode I fracture toughness of flexible bonded joints. Eng Fract Mech 2019;218:106584. http://doi.org/10.1016/j.engfracmech.2019.106584

23. Rosendahl PL, Staudt Y, Odenbreit G, Schneider J, Becker W. Measuring mode I fracture properties of thick-layered structural silicone sealants. Int J Adhes Adhes 2019;91:64-71. http://doi.org/10.1016/j.ijadhadh.2019.02.012
24. Yamagata Y, Lu X, Sekiguchi Y, Sato C. Experimental investigation of mode I fracture energy of adhesively bonded joints under impact loading conditions. Appl Adhes Sci 2017;5:7. http://doi.org/10.1186/s40563-017-0087-7
25. Lißner M, Alabort E, Erice B, Cui H, Blackman BRK, Petrinic N. On the dynamic response of adhesively bonded structures. Int J Impact Eng 2020;138:103479. http://doi.org/10.1016/j.ijimpeng.2019.103479
26. Sekiguchi Y, Yamagata Y, Sato C. Mode I fracture energy of adhesive joints bonded with adhesives with different characteristics under quasi-static and impact loading. J Adhes Soc Jpn 2017;53(10):330-7. http://doi.org/10.11618/adhesion.53.330
27. Komatsu K, Sekiguchi Y, Ihara R, Tatsumi A, Sato C. Experimental investigation of an adhesive fracture energy measurement by preventing plastic deformation of substrates in a double cantilever beam test. J Adhes 2019; 95(10):911-28. http://doi.org/10.1080/00218464.2018.1451332
28. Abe N, Sekiguchi Y, Sato C. Parameter identification of material model of toughened adhesive polymer for elasto-plastic finite element analysis. J Adhes Soc Jpn 2018;54(10):358-66. http://doi.org/10.11618/adhesion.54.358
29. Adhesives – Determination of the mode 1 adhesive fracture energy of structural adhesive joints using double cantilever beam and tapered double cantilever beam specimens. ISO 25217:2009.
30. Williams JG. The fracture mechanics of delamination tests. J Strain Analysis 1989;24(4):207-13. http://doi.org/10.1243/03093247v244207
31. Sekiguchi Y, Hayashi A, Sato C. Analytical determination of adhesive layer deformation for adhesively bonded double cantilever beam test considering elastic-plastic deformation. J Adhes 2020;96(7):647-64. http://doi.org/10.1080/00218464.2018.1489799
32. Pardoen T, Ferracin T, Landis CM, Delannay F. Constraint effects in adhesive joint fracture. J Mech Phys Solids 2005;53:1951-83. http://doi.org/10.1016/j.jmps.2005.04.009
33. Kamiyama K, Mikuni M, Matsumoto T, Matsuda S, Kishi H. Crack growth mechanism on SGA

adhesive joints. Int J Adhes Adhes 2020;103:102690. http://doi.org/10.1016/j.ijadhadh.2020.102690